Spectroscopy 17 (2003) 435–445
IOS Press

Raman spectroscopy of regulatory protein Omega from *Streptococcus pyogenes* plasmid pSM19035 and complexes with operator DNA

Lubomír Dostál [a], Rolf Misselwitz [a], Stefan Laettig [a], Juan C. Alonso [b] and Heinz Welfle [a,*]

[a] *Max-Delbrueck-Centrum fuer Molekulare Medizin Berlin-Buch, Robert-Roessle-Str. 10, D-13092 Berlin, Germany*

[b] *Departmento de Biotecnología Microbiana, Centro Nacional de Biotecnología, C.S.I.C., E-28049, Madrid, Spain*

Abstract. pSM19035-encoded homodimeric ω protein (ω_2) regulates transcription of genes required for control of plasmid copy number and stable inheritance. ω_2 belongs to the MetJ/Arc structural superfamily of repressors forming a ribbon-helix-helix (RHH) DNA binding motif, and binds specifically to operator regions containing at least two consecutive copies of heptad sequences 5′-$^{A}/_{T}$ATCAC$^{A}/_{T}$-3′ in direct or inverted orientation. Solution properties of a double stranded 19 base-pairs oligonucleotide designed to model an operator DNA binding site of ω_2 (top strand 5′-GCG AATCACA TGTGATT GG-3′), ω_2, and the ω_2:19-bp DNA complex were analysed by Raman spectroscopy. The Raman data indicate a sequence specific induced fit of both interacting macromolecules with ω_2 binding to the major groove of the DNA, large perturbations of the DNA attributable to base unstacking, changes in vibrational modes of deoxyribose moieties, and protein-induced DNA bending. Protein marker bands indicate that α-helices are preserved, whereas amino acid side chains are largely perturbed, and unordered structures and turns become extensively restructured. Raman difference bands are consistent with interactions of thymine, adenine and cytosine with ω_2 side chains. The results suggest that the central TCA/TGA stretch of the heptads might be the main target site for ω_2 binding to operator DNA.

1. Introduction

Plasmid pSM19035 from *Streptococcus pyogenes* is a member of the *inc*18 family of low-copy-number and broad-host-range plasmids from Gram-positive bacteria. The pSM19035-encoded ω protein directly represses transcription of *cop*S, δ and ω genes and indirectly controls expression of the ε and ζ genes [1]. These genes are required for copy number control and stable maintenance of plasmids. Thus, ω protein is a global regulator actively engaged in these functions [1].

The ω protein is composed of 71 amino acid residues, and occurs as homodimer in solution (ω_2, molecular mass 16 kDa) with a K_d of 3.2 μM and mainly α-helical (42%) folding. ω dimer unfolds and refolds reversibly depending on urea concentration, and unfolds thermally with half transition temperatures, T_m, between ∼43 and ∼78°C depending on the ionic strength of the buffer [2]. In crystals, two ω monomers related by a non-crystallographic 2-fold rotation axis form a homodimer ω_2 that occupies the asymmetric

*Corresponding author: Dr. Heinz Welfle, Max-Delbrück-Centrum für Molekulare Medizin, Postfach 740238, D-13092 Berlin, Germany. Fax/Tel.: +49 30 9406 2840; E-mail: welfle@mdc-berlin.de.

unit. Each ω monomer is folded into one β-strand and two helices. In the dimer the β-strands form an antiparallel β-ribbon, and the α-helices are intertwined to a hydrophobic core structure. The ω protein belongs to the structural superfamily of MetJ/Arc repressors featuring a ribbon-helix-helix (RHH) DNA binding motif [3]. Proteins of this family recognise the major groove of DNA with the β-ribbon of the RHH motif.

ω_2 binds specifically and with high affinity to multiple 7-bp repeats (5′-$^{A}/_{T}$ATCAC$^{A}/_{T}$-3′, top strand of the consensus motif) located immediately upstream and within the promoter (P) regions in the upstream operator regions of *cop*S and δ genes and of the ω-ε-ζ operon. The 7-bp repeats are arranged in different modes in $P\delta$, $P\omega$ and P*cop*S, e.g. in $P\omega$ in two copies of a block with two direct and one inverted 7-bp repeat, and one inverted 7-bp repeat downstream of the block $[(\rightarrow)_2(\leftarrow)]_2(\leftarrow)$. At least two consecutive copies of the 7-bp consensus repeat are necessary for cooperative high affinity binding of ω_2.

In the present study, we analyse by Raman spectroscopy the binding of ω_2 to a 19-bp DNA segment modelling an operator binding site of ω_2. The 19-bp DNA is composed of two heptads in direct and inverted orientation flanked by unspecific base-pairs (top strand: 5′-GCG AATCACA TGTGATT GG-3′). The flanking base-pairs are intended to stabilise the duplex and to reduce fraying of 5′- and 3′-terminal base-pairs. The 19-bp DNA binds two ω_2 dimers. The Raman difference spectrum obtained by subtraction of the sum of spectra of isolated ω_2 and DNA from the spectrum of the complex reveals a number of Raman marker bands specific to the ω_2:DNA complex.

2. Experimental

2.1. Chemicals

Isopropyl-β-D-thiogalactopyranoside (IPTG) and rifampicin were obtained from Roth, Karlsruhe, Germany and Fluka, Deisenhofen, Germany, respectively. Ultrapure acrylamide was from Serva, Heidelberg, Germany. All other chemicals were purchased from Merck, Darmstadt, Germany. Phosphocellulose was from Whatman, Maidstone, UK. Superose 12, SP-sepharose, heparin-sepharose and Mono Q were from Amersham-Pharmacia, Freiburg, Germany.

2.2. Preparation of ω protein

The ω gene was overexpressed in *E. coli* BL21(DE3) cells carrying plasmid pT712ω, after induction with IPTG and addition of rifampicin, and its product purified as described [2]. Prior to spectroscopic measurements, ω protein was extensively dialysed against 50 mM Tris-HCl pH 7.5, 50 mM NaCl and 10 mM $MgCl_2$, passed through 0.22 μ Millipore filters, and concentrated. Protein concentrations were determined from the absorbance at 276 nm using an absorption coefficient of $A_{1\%,\ 1\ cm} = 3.63$ [2].

2.3. Preparation of DNA and ω_2:DNA complex

Oligonucleotides were purchased from the Department of Functional Genomics and Proteomics of the Masaryk University Brno, Czech Republic. The sequences of 19-bp operator DNA model and 19-bp oligonucleotide used as unspecific reference DNA (molecular masses 11 600 Da) are shown in Fig. 1. Concentrations of both DNAs were determined spectrophotometrically using the same extinction coefficient $\varepsilon_{260\ nm} = 12\,978\ M\,bp^{-1}\,cm^{-1}$ calculated from the base composition according to [4].

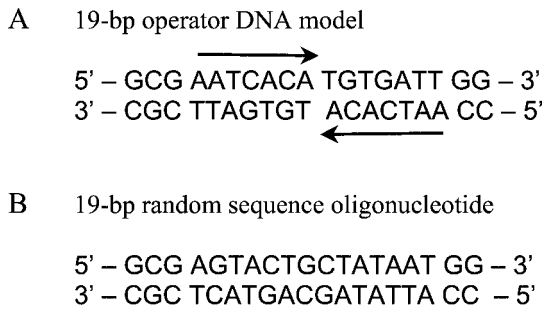

Fig. 1. Nucleotide sequences of the two oligonucleotides used in this study. (A). 19-bp oligonucleotide designed as operator DNA model with one heptad in direct and a second heptad in indirect orientation indicated by arrows, and three and two flanking base-pairs. (B) 19-bp oligonucleotide with the same base-pair composition as the operator DNA model but with random sequence instead of ω_2 binding heptads.

Equimolar amounts of each strand were mixed, annealed at 95°C and purified by ion exchange chromatography on a Mono Q HR 5/5 column using a linear gradient of 0.05 to 1 M NaCl in 50 mM Tris-HCl buffer pH 7.5. Peak fractions were exhaustively dialysed against water and lyophilised.

The complex of ω_2 with the 19-bp operator DNA (briefly ω_2:DNA) was prepared by mixing appropriate amounts of the components dissolved in 50 mM Tris-HCl pH 7.5, 50 mM NaCl and 10 mM $MgCl_2$ to produce a 2 : 1 molar ratio of ω dimer to 19-bp operator DNA. A mixture of ω_2 with the 19-bp DNA with random sequence was prepared in the same way to produce the same 2 : 1 molar ratio and analysed as a reference for non-interacting components. The samples were concentrated in a Millipore Ultrafree centrifugal filter device. ω_2:DNA complex formation was controlled by 12.5% (w/v) non-denaturing PAGE in TEB buffer as previously described [1].

2.4. Raman spectroscopy

Samples of approximately 15 μl were sealed in homemade cuvettes consisting of cylindrical quartz bodies with quartz bottoms and Teflon stoppers. The concentrations were about 50 mg/ml for DNA, 85 mg/ml for ω_2, 190 mg/ml for the ω_2:DNA complex and 140 mg/ml for the mixture of ω_2 with 19-bp DNA with random sequence. Raman spectra were excited with the 488-nm line of a Coherent Innova 90 argon laser. The measurements were repeated with 514.5-nm excitation, with excitation energy at sample space of approximately 100 mW at both wavelengths. Spectra were collected at 22°C on the Raman spectrometer T64000 (Jobin Yvon, France) equipped with a liquid nitrogen-cooled charge-coupled-device (CCD) detector. 6 spectra of 120 s each were accumulated and averaged.

Raman data analyses, including all spectra manipulations described below, were performed with the software packages LabSpec (Jobin Yvon) and GRAMS (Thermo Galactic). Solution spectra were corrected by subtraction of the buffer spectrum and fluorescence background that was approximated by a polynomial curve. For calculation of the difference spectrum, at first the spectra of isolated components were normalised with respect to the Raman band near 1092 cm^{-1} to minimise intensity differences to the spectrum of ω_2:DNA. The 1092 cm^{-1} band is assigned to the P–O stretching vibration of the phosphodioxy group (PO_2^-) and was shown to be invariant upon repressor protein binding to operator DNA [5]. Then, the normalised but not otherwise corrected experimental spectra of 19-bp DNA and ω_2 were subtracted from the spectrum of the ω_2:DNA complex. In the next steps the buffer spectrum and finally, fluorescence background were removed.

Difference bands are considered as significant when the following criteria are fulfilled: (i) their intensity is at least two times higher than the signal-to-noise ratio, and (ii) the difference bands reflect intensity changes of at least 5% of their parent bands.

3. Results

3.1. Raman spectrum of the 19-bp operator DNA

Figure 2 shows the Raman spectrum of the 19-bp operator DNA in the 600–1720 cm^{-1} wavenumber region. Wavenumber positions of the major peaks are given in the figure. The backbone conformation markers at 838 and 1094 cm^{-1} are diagnostic of B-DNA [6], and the nucleoside conformation markers at 671 cm^{-1} (dT), 683 cm^{-1} (dG), 730 cm^{-1} (dA), 753 cm^{-1} (dT), 1258 cm^{-1} (dC) identify C2′-endo/anti-conformers. This spectrum is the signature of the operator site model with two heptads in direct and inverted orientation and provides the basis for the interpretation of the difference spectrum. Peak assignments are summarised in Table 1.

3.2. Raman spectrum of ω dimer

Figure 3 shows the Raman spectrum of ω_2. Wavenumber positions of the major peaks are given in the figure, and peak assignments of amide I (1640–1680 cm^{-1}) and amide III bands (1230–1300 cm^{-1}), bands of aromatic and nonaromatic amino acids and the α-helical skeletal mode ($\sim$934 cm^{-1}) are summarised in Table 1.

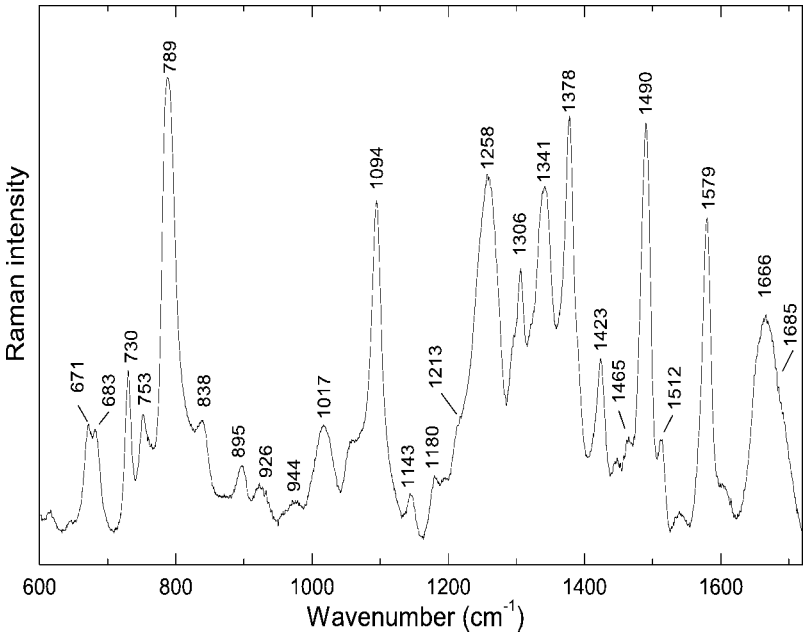

Fig. 2. Raman spectrum of 19-bp oligonucleotide designed as operator DNA model (sequence see Fig. 1, A) in the region 600–1720 cm^{-1}. Sample buffer is 50 mM Tris-HCl pH 7.5, 50 mM NaCl and 10 mM $MgCl_2$; data were collected at 22°C. Peak positions of prominent Raman bands are labeled and listed in Table 1.

Table 1
Raman frequencies and assignments for 19-bp operator DNA and ω dimer

19-bp operator DNA		ω dimer	
frequency (cm^{-1})	assignment	frequency (cm^{-1})	assignment
671	Thy	644	Y
683	Gua	698	M
730	Ade	724	Y, M
753	Thy	750	I, L, K (CH_2 rock); A (CH_3 rock)
789	Cyt, bk	834	Y
838	bk (OPO)	852	Y
895	bk	898	A
926	bk	940	skeletal mode α-helix
944	bk	958	(CH_3 symmetric rock)
1017	Gua, Thy	990	I (C–C stretch)
1094	bk (PO_2^-)	1025	Y
1143	Thy	1040	S, T, D, E (C–O stretch); P (C–N stretch)
1180	Thy, Cyt	1060	K, A (C–C stretch)
1213	Thy	1102	P (C–N stretch); A (C–C stretch)
1258	Thy, Cyt	1129	I, V, L (C–C stretch)
1306	Ade, Cyt	1159	V, I, (C–C stretch)
1341	Ade, Gua	1174	Y; CH_3 symmetric rock
1378	Thy	1210	Y
1423	bk	1237	amide III
1465	bk	1255	amide III
1490	Gua, Ade	1276	amide III
1512	Ade	1318	(CH_2 twist/wag)
1579	Gua, Ade	1342	(CH_2 twist/wag)
1666	Thy	1401	(COO^- symmetric stretch)
1685	Gua	1425	(CH_2, CH_3 deformation)
		1447	(CH_2 scissors)
		1462	A, V (CH_3 asymmetric bend) L, I (CH_2 scissors)
		1618	Y
		1656	amide I
		1673	amide I

Frequencies (cm^{-1}) are accurate to within ± 3 cm^{-1}. Abreviations and notations are as follows: Gua, guanine; Thy, thymine; Cyt, cytosine; Ade, adenine; bk, deoxyribose backbone; OPO, phosphodiester backbone group; PO_2^-, phosphodioxy backbone group; one-letter code is used for amino acids; CH_2, methylene; CH_3, methyl; C–C, carbon–carbon bond; C–N, carbon–nitrogen bond; C–O, carbon–oxygen bond. Brackets indicate chemical group frequencies common to more than one type of side chains. Assignments according to recent studies [13–16].

3.2.1. Secondary structure of ω dimer

Positions of the amide I and amide III bands are diagnostic of α-helix and irregular conformations as the principle types of secondary structure of ω_2. The prominent amide I and amide III components centred near 1656 and 1276 cm^{-1}, respectively, as well as the intense C–C stretch band at 940 cm^{-1} and the intense band at 1342 cm^{-1} indicate a high content of α-helices. The amide III peak near 1237 cm^{-1} and the shoulder of the amide I band near 1673 cm^{-1} indicate the presence of some β-structures. Turns and irregular conformations are indicated by the amide III band near 1255 cm^{-1} and contribute to the amide I peak [7]. The Raman data are consistent with CD measurements [2] and the X-ray crystal structure of ω_2

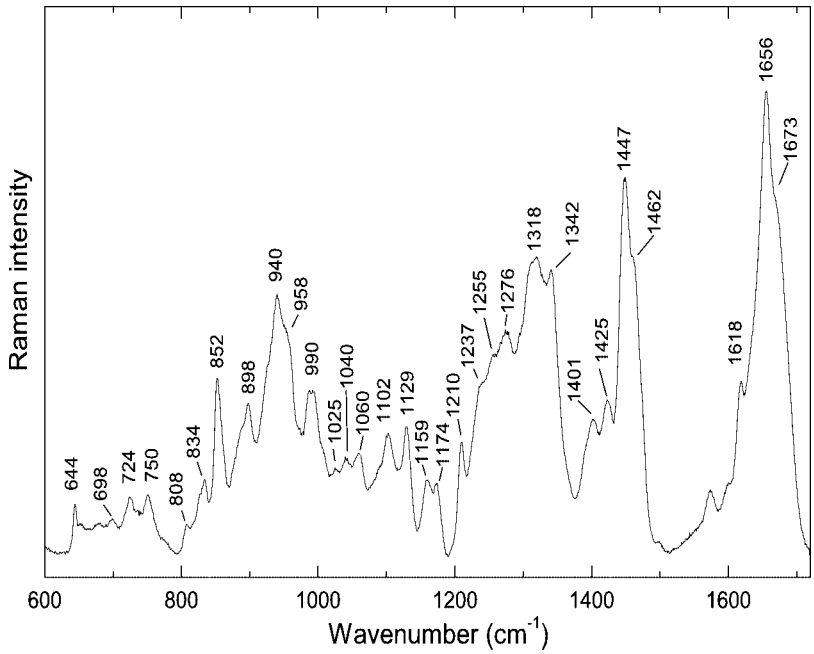

Fig. 3. Raman spectrum of ω dimer in the region 600–1720 cm^{-1}. Sample buffer is 50 mM Tris-HCl pH 7.5, 50 mM NaCl and 10 mM $MgCl_2$; data were collected at 22°C. Peak positions of prominent Raman bands are labeled by the respective wavenumbers and listed in Table 1.

in which N-terminal amino acids 1–23 and 1′–22′ [3] could not be located in the electron density map as they are disordered [3].

3.2.2. Environment of tyrosine side chains

A tyrosine doublet at ∼850 and ∼830 cm^{-1} is caused by Fermi resonance of the normal mode ν_1 (ring breathing fundamental) and the second harmonic $2\nu_{16a}$ (ring deformation overtone) of the para-substituted phenolic side chain [8]. The intensity ratio I_{850}/I_{830} is an indicator of the tyrosine environment as it is sensitive to hydrogen bonding of phenolic OH groups [8]. The Fermi doublet of the four tyrosines of ω_2, Y62, Y66, Y62′, Y66′, has peaks at 852 cm^{-1} and 834 cm^{-1} with an intensity ratio of 2.3. This indicates that tyrosine hydroxyls of ω_2 are acceptors of strong hydrogen bonds formed with very acidic hydrogens of proton donors [8].

3.3. Raman analysis of the ω_2:DNA complex

The Raman spectrum of the ω_2:DNA complex is shown in the top of Fig. 4 (trace 1). Figure 4, trace 2 represents the computed sum of the separately measured spectra of isolated components, shown in Figs 2 and 3. Figure 4, trace 3 is the difference spectrum obtained by subtraction of the sum of component spectra from the spectrum of the complex (trace 1 minus trace 2), and trace 5 is the 3-fold amplified difference spectrum. A positive difference peak indicates an increased Raman intensity at the respective wavenumber region in the spectrum of the complex compared to the spectrum of the sum of component spectra, and a negative trough is caused by a lower intensity in the spectrum of the complex.

For comparison, Fig. 4 shows a difference spectrum (trace 4) obtained by subtraction of the sum of component spectra from the spectrum of a mixture of ω_2 with the random sequence 19-mer but the same

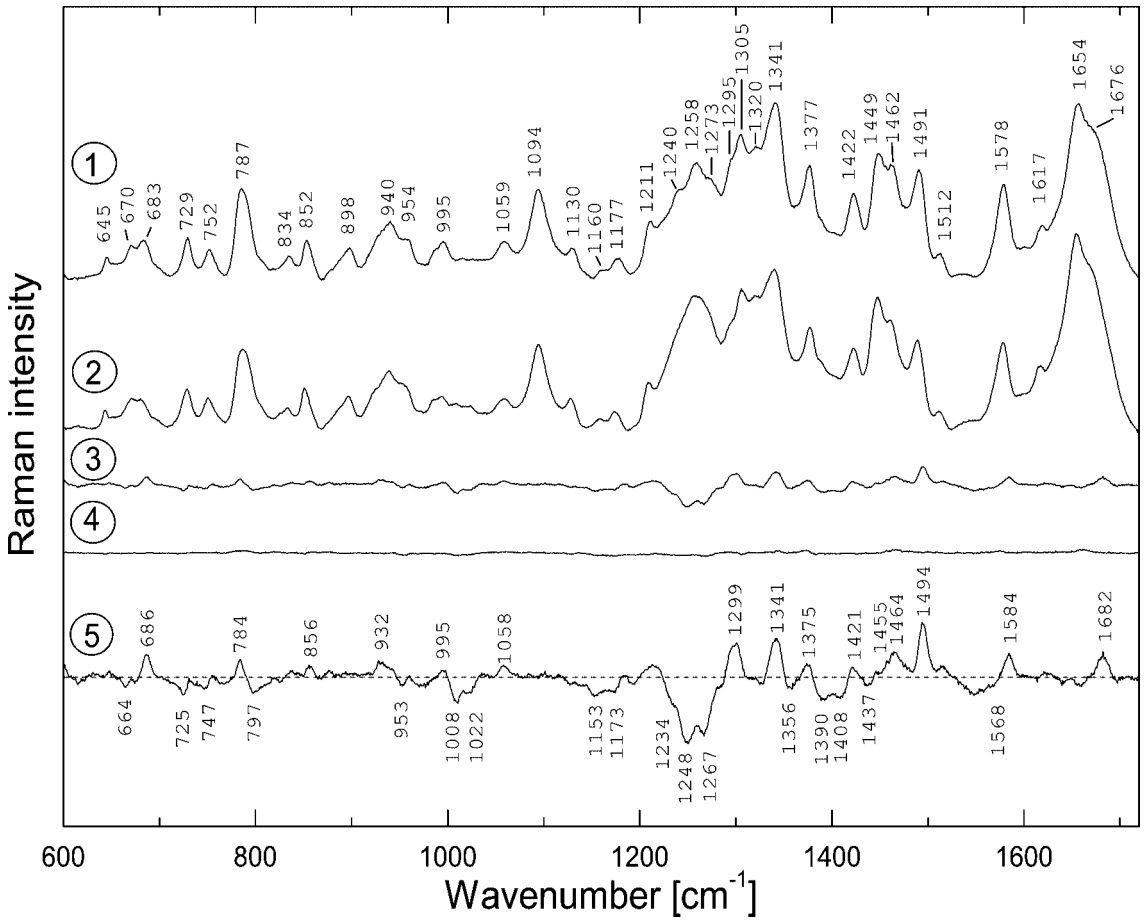

Fig. 4. Raman spectrum of ω dimer in complex with 19-bp operator DNA (ω_2:DNA) in the region 600–1720 cm^{-1} (trace 1). Trace 2 shows the spectral sum of the isolated component spectra shown in Figs 2 and 3. Trace 3 shows the computed difference spectrum obtained by subtraction of the sum of the isolated component spectra from the spectrum of ω_2:DNA (trace 1 minus trace 2). Trace 4 shows the computed difference spectrum obtained by subtraction of the sum of the isolated component spectra from the experimental spectrum of a mixture of ω_2 with the 19-bp random sequence oligonucleotide (Fig. 1, B). Trace 5 shows the the difference spectrum of ω_2:DNA in 3-fold amplification of trace 3.

base composition as the 19-bp operator DNA (see Fig. 1). The practically featureless trace 4 indicates that ω_2 and random sequence 19-mer have the same Raman spectra in isolated form and in the mixture. ω_2 and unspecific DNA do not interact even at the high concentrations used for the Raman measurement.

Contrarily, many intensive difference bands for the ω_2:DNA complex are visible in trace 3 and in enlarged form in trace 5 of Fig. 4. These difference bands indicate large changes in the Raman signatures of ω_2 and 19-bp operator DNA as a consequence of complex formation. The difference spectrum provides information about interactions that accompany structural rearrangements and dramatic conformational changes associated with binding. Some of the difference bands are assignable to separate vibrations of the components; overlapping of DNA and protein bands causes other difference bands.

3.3.1. Effects of complex formation on Raman bands of 19-bp operator DNA

Backbone and deoxynucleoside conformation. The 600–900 cm^{-1} region contains Raman markers of deoxynucleoside conformation and DNA backbone geometry [6]. One difference peak at 686 cm^{-1} and

two troughs at 664 and 725 cm^{-1} indicate an altered deoxynucleoside conformation in the complex (Fig. 4, trace 5). A peak at 683 cm^{-1} in Raman spectra of DNA is a guanosine nucleoside conformation marker for B-form DNA. The difference peak at position 686 cm^{-1} indicates an increased intensity of the dG vibration in the complex and points to a change in the B-DNA geometry. The troughs at 664 and 725 cm^{-1} result from reduced intensities of peaks assigned to dT (671 cm^{-1}) and dA (730 cm^{-1}). In Raman spectra of DNA the cytosine peak at 782 cm^{-1} overlaps a backbone component around 794 cm^{-1} which is assigned to a stretching vibration of backbone phosphodiester groups and diagnostic of B-form DNA backbone geometry, specifically of torsions angles α and ζ in gauche$^-$ range [9]. The derivative feature in trace 5 near 790 cm^{-1} with difference peak and trough at 784 and 797 cm^{-1}, respectively, points to an intensity change of the dC vibration at 782 cm^{-1} and to a shift to lower wavenumber of the 794 cm^{-1} B-form marker.

Deoxyribose ring vibrations. The difference peak near 932 cm^{-1} but also the derivative feature with trough at 1408 cm^{-1} and difference peak at 1421 cm^{-1} reveal perturbations of Raman bands assigned to furanose ring vibrations [10] and indicate ω_2 interactions with deoxyribose sites. This is supported by a small derivative feature with trough at 1437 cm^{-1} and 1455 cm^{-1} shoulder of the intense and wide 1464 cm^{-1} difference peak caused by ω_2 vibrations. Bands around 1419 and 1455 cm^{-1} are assigned to CH_2 scissoring modes of C5′H_2 and C2′H_2 groups, respectively. The derivative features found near 1419 and 1450 cm^{-1} indicate wavenumber changes of the 1419 and 1455 cm^{-1} bands and suggest alterations of the DNA helix geometry as induced by bending and/or unwinding [9].

Raman markers of base environment and interaction. Raman bands in the interval 1300–1750 cm^{-1} are sensitive to specific interactions between DNA bases and major groove-binding proteins [11–14]. The prototype Raman marker of protein–DNA interaction in the major groove is the guanine band near 1490 cm^{-1}. This band shifts to near 1470 cm^{-1} upon hydrogen bond donation to the N7 guanine ring acceptor [5,10,11,14], resulting in a characteristic derivative band profile with difference peak at $\sim$1470 cm^{-1} and trough at $\sim$1490 cm^{-1}. Such a derivative band profile is clearly missing in the difference spectrum of the ω_2:DNA complex. Instead, there are two large difference peaks at 1464 and 1494 cm^{-1}. The 1464 cm^{-1} difference peak could be caused, at least in part, by an increase of the Raman intensity because of guanine N7 hydrogen bond formation and concomitant shift of the 1490 cm^{-1} guanine band to shorter wavenumbers. In this case a reduction of the peak intensity at $\sim$1490 cm^{-1} would follow and should result in a trough of the difference spectrum. However, the actually observed large difference peak at 1490 cm^{-1} indicates that unstacking of purines and not guanine N7 bond formation dominates the Raman features of the difference spectrum in this region. Unstacking results in a large intensity increase of the 1490 cm^{-1} band assigned to adenine and guanine, and a difference peak at 1494 cm^{-1} was interpreted as an indicator of purine unstacking [9,13]. The large intensity increase of the 1490 cm^{-1} peak caused by unstacking could overlap an intensity reduction caused by guanine N7 hydrogen bond formation. Therefore, the features in this region of the difference spectrum do not provide conclusive evidence for guanine N7 hydrogen bond formation but formally do not exclude it.

A further Raman marker for major groove binding of proteins is a trough at 1717 cm^{-1} attributed to guanine O6 interactions [5,11]. Such a difference band is not observed for the ω_2:DNA complex, neither in difference spectra obtained from measurements with 488 nm laser line excitation (Fig. 4) nor from those with 514.5 nm excitation (data not shown).

The adenine and guanine Raman marker bands at $\sim$1341 and $\sim$1579 cm^{-1} exhibit large effects upon ω_2 binding. Difference peaks at 1341 and 1584 cm^{-1} are indicative of purine unstacking. In addition to unstacking, small troughs at 1356 and 1568 cm^{-1} indicate shifts of the 1341 and 1579 cm^{-1} peaks

assigned to guanine and adenine because of contacts with ω_2. Interaction of ω_2 with guanine should have its largest effect at the 1490 cm^{-1} band as discussed above. Since there evidence is missing for ω_2 binding to guanine, we propose that the derivative features near 1341 and 1579 cm^{-1} are mainly caused by ω_2 interactions with the adenine moiety.

The Raman peak at 1378 cm^{-1} is assigned to the thymine exocyclic $C5H_3$ group. Intensity increase of this band is correlated with increased hydrophobicity in the surrounding of thymine $C5H_3$ groups, as observed in repressor–DNA complexes where the thymine $C5H_3$ groups are shielded by hydrophobic side chains of the bound repressor [5,14]. The difference spectrum of ω_2:DNA complex shows a derivative feature with difference peak and trough near 1375 and 1390 cm^{-1}, respectively. For the hSRY-HMG:DNA system similar features were observed but so far not definitely interpreted, although protein contacts are considered as possibly responsible [9].

The troughs at 1008 and 1022 cm^{-1} may be caused by effects of complex formation on guanine and thymine but up to now are not further assignable.

3.3.2. Effects of complex formation on Raman bands of ω dimers

Tyrosine. Several peaks of the difference spectrum are assignable to tyrosine. A difference peak at 856 cm^{-1} indicates an increase of the 852 cm^{-1} band of the tyrosine Fermi doublet while the intensity of the 834 cm^{-1} band remains constant. This increases the I_{852}/I_{834} ratio of the complex in comparison to that of the isolated ω dimer. Assuming that only tyrosines contribute to the 852 cm^{-1} band, the average hydrophobicity of the tyrosine environment in the complex is increased. The intensity of the tyrosine CH_3 symmetric rock Raman band is decreased in the complex (trough at 1173 cm^{-1}). Tyrosine may contribute to the large trough at 1267 cm^{-1} that is mostly caused by changes in amide III vibrations (discussed below).

Side chains of nonaromatic amino acids. The difference spectrum of ω_2:DNA reveals perturbations in Raman bands of nonaromatic amino acids (C–C or/and C–N stretch, CH_2 and CH_3 vibrations) [15]. Relevant features are a trough at 747 cm^{-1} (assigned to leucine and lysine CH_2 rock), a trough at 953 cm^{-1} (CH_3 symmetric rock), a difference peak at 1058 cm^{-1} (C–O stretch of serine, threonine, glutamic acid and aspartic acid, C–C stretch of alanine and lysine, C–N stretch of proline), a trough at 1153 cm^{-1} (C–C stretch of valine and isoleucine), and difference peaks at 1341 cm^{-1} (lysine CH_2 twist/rock and alanine CH_2 bend) and 1464 cm^{-1} (C–C stretch).

Secondary structure of ω_2. The difference spectrum of ω_2:DNA reveals the largest differences in the region between 1200 and 1320 cm^{-1} where the intensive amide III bands of ω_2 overlap with the wide, intense 1258 cm^{-1} band of cytosine and thymine (CT band) of the 19-bp operator DNA. Thus, the observed spectral features of the difference spectrum may be caused by protein, DNA or both components of the complex. The situation is similar in the 1640–1690 cm^{-1} region, where the intensive amide I protein bands overlap with guanine and thymine bands. Therefore, the interpretation of secondary structure changes of ω_2 has to consider possible contributions from DNA in the difference features of the amide III and amide I regions.

In the 1200–1320 cm^{-1} region are 3 troughs around 1234, 1248, and 1267 cm^{-1} and one difference peak around 1299 cm^{-1}. The 1234 cm^{-1} trough could be caused by diminished intensity of the amide III band at 1237 cm^{-1} assigned to β-structures and/or by changes in the CT band. It is possible but unlikely that the 1299 cm^{-1} difference peak and the trough at 1267 cm^{-1} are caused by a shift of the 1273 cm^{-1} amide III band to larger wavenumbers. The 1273 cm^{-1} band is assigned to α-helices and changes would point to an increased α-helix content. However, an increase of α-helical content is not supported by other features of the difference spectrum (no difference features in the amide I region at the 1656 cm^{-1}

α-helix position and at the 940 cm^{-1} Raman band assigned to the skeletal mode of α-helices). Alternatively, increased intensity of the adenine and guanine band at 1306 cm^{-1} due to purine unstacking may contribute to the 1299 cm^{-1} difference peak. As already mentioned, tyrosine may contribute to the trough at 1267 cm^{-1}. Changes in irregular structures and turns should cause Raman difference features around 1255 cm^{-1} where an amide III band is assigned to random coil structures. Actually, the most prominent trough of the ω_2:DNA difference spectrum is located at 1248 cm^{-1}. A decrease of the 1248 cm^{-1} band of the complex is consistent with the structuring of the about 20 N-terminal amino acids per ω chain which are probably unfolded in solution [2,3].

At the α-helix position of the amide I region around 1656 cm^{-1} the difference spectrum is featureless and does not indicate changes in the content of α-helices upon complex formation. However, an increase of the amide I component assigned to turns and irregular structure may largely contribute to the difference peak at 1682 cm^{-1}. This result supports the structuring of the N-terminal amino acids of ω_2 in the complex. In addition, the difference peak at 1682 cm^{-1} may in part reflect an increase of the 1685 cm^{-1} peak associated with guanine unstacking.

4. Discussion

This study represents a first attempt to characterise the interaction of ω_2 with its operator DNA by means of Raman spectroscopy. We analysed spectra of ω_2, 19-bp operator DNA carrying two 5′-AATCACA-3′ heptads (top strand) in direct and inverted orientation, and ω_2:DNA complex. A Raman difference spectrum is obtained by subtraction of the sum of the spectra of isolated components from the spectrum of ω_2:DNA. The difference spectrum shows surprisingly large spectral features suggesting an induced fit of ω_2 and operator DNA upon complex formation with substantial conformational changes of both components. In contrast, the Raman spectrum of a mixture of ω_2 with a 19-bp random sequence DNA hardly indicates interactions or conformational changes, as demonstrated by a nearly featureless difference spectrum (spectrum of mixture minus sum of component spectra).

Protein–DNA complexes studied by Raman spectroscopy provide examples for major groove binding, minor groove binding, and interaction with single stranded DNA [5,9–14]. Recently, Raman markers of different protein/DNA recognition motifs were proposed [13]. Comparison of features of the ω_2:DNA difference spectrum with the list of proposed Raman markers reveals that the properties of the ω_2:DNA complex are only partly represented by the complexes studied so far.

Raman difference bands assignable to DNA backbone and diagnostic of minor groove binding are not present in the ω_2:DNA difference spectrum. In contrast, bands proposed to be diagnostic of minor groove binding and assignable to thymine and purine unstacking are present. These Raman markers were derived from studies of the hSRY-HMG:DNA complex [9]. The structure of this complex is characterised by minor groove binding of the hSRY-HMG protein with expansion of the minor groove, sharp bending toward the major groove, and local unwinding of the double helix.

The difference peak at 1375 cm^{-1} in the ω_2:DNA difference spectrum assignable to shielding of thymine $C5H_3$ belongs to the Raman marker bands diagnostic for major groove binding [13]. However, in the ω_2:DNA difference spectrum Raman marker bands are not detectable that are characteristic for guanine N7 and O6 hydrogen bond formation and provide the most characteristic difference features for major groove binding in repressor–DNA complexes [5,11,12,14].

We conclude that ω_2 binds to the major groove of the operator DNA and induces unstacking of bases, preferably A, T and C and also G, but interaction with G bases is weak or below the detection limits.

Major groove binding of ω_2 was proposed earlier because of its structural homology with members of the Arc/MetJ protein family [3].

Changes in Raman marker bands assigned to amino acid side chains, amide III and amide I bands indicate restructuring of turns and unordered structures of ω_2 and imply DNA-dependent reorganization of the ω_2 tertiary structure, suggesting an active participation of the N-terminal amino acid sequences in DNA binding. The extent of changes of Raman markers assigned to protein side chains is large enough to account also for ω_2–ω_2 interactions in the complex which are expected because of the cooperative binding of ω_2 to *cop*S DNA [1]. The tyrosine residues of ω_2 (Y61, Y66, Y61′, Y66′) are localised in helices B and B′ [3] that are far from the proposed DNA binding site. The difference features assigned to tyrosine suggest global changes in the protein structure upon DNA binding. The preservation of α-helices in the complex, however, indicates that dominant structural elements of ω_2, present in isolated protein, are utilised in the process of complex formation.

Modified operator DNA models with different orientation and/or different number of heptads will be used in further Raman studies for a detailed analysis of the respective complexes.

Acknowledgement

This research was partly supported by grant BMC2000-0548 from MCT-DGI to J.C.A., by Deutsche Forschungsgemeinschaft (Graduiertenkolleg 80/2 and We1745/5-1) to H.W., and by the EU (QLK3-CT-2001-00277) to J.C.A. and H.W. We thank Dr. W. Saenger for stimulating discussions and critical reading of the manuscript.

References

[1] A.B. de la Hoz, S. Ayora, I. Sitkiewicz, S. Fernandez, R. Pankiewicz, J.C. Alonso and P. Ceglowski, *Proc. Natl. Acad. Sci. USA* **97** (2000), 728–733.
[2] R. Misselwitz, A.B. de la Hoz, S. Ayora, K. Welfle, J. Behlke, K. Murayama, W. Saenger, J.C. Alonso and H. Welfle, *FEBS Lett.* **505** (2001), 436–440.
[3] K. Murayama, P. Orth, A.B. de la Hoz, J.C. Alonso and W. Saenger, *J. Mol. Biol.* **314** (2001), 789–796.
[4] V.A. Bloomfield, D.M. Crothers and I. Tinoco, Jr., Electronic and vibrational spectroscopy, in: *Nucleic Acids, Structures, Properties, and Functions*, University Science Books Sausalito, California, 1999, pp. 165–221.
[5] J.M. Benevides, M.A. Weiss and G.J. Thomas, Jr., *Biochemistry* **30** (1991), 5955–5963.
[6] G.J. Thomas, Jr. and A.H.-J. Wang, *Nucleic Acids Mol. Biol.* **2** (1988), 1–30.
[7] W.L. Peticolas, *Meth. Enzymol.* **246** (1995), 389–416.
[8] M.N. Siamwiza, R.C. Lord, M.C. Chen, T. Takamatsu, I. Harada, H. Matsuura and T. Shimanouchi, *Biochemistry* **14** (1975), 4870–4876.
[9] J.M. Benevides, G. Chan, X.-J. Lu, W.K. Olson, M.A. Weiss and G.J. Thomas, Jr., *Biochemistry* **39** (2000), 537–547.
[10] G.J. Thomas, Jr., J.M. Benevides, S.A. Overman, T. Ueda, K. Ushizawa, M. Saitoh and M. Tsuboi, *Biophys. J.* **68** (1995), 1073–1088.
[11] J.M. Benevides, M.A. Weiss and G.J. Thomas, Jr., *Biochemistry* **30** (1991), 4381–4388.
[12] J.M. Benevides, M.A. Weiss and G.J. Thomas, Jr., *J. Biol. Chem.* **269** (1994), 10 869–10 878.
[13] J.M. Benevides, T. Li, X.-J. Lu, A.R. Srinivasan, W.K. Olson, M.A. Weiss and G.J. Thomas, Jr., *Biochemistry* **39** (2000), 548–556.
[14] C. Krafft, W. Hinrichs, P. Orth, W. Saenger and H. Welfle, *Biophys. J.* **74** (1998), 63–71.
[15] S.A. Overman and G.J. Thomas, Jr., *Biochemistry* **38** (1999), 4018–4027.
[16] S.A. Overman and G.J. Thomas, Jr., *Biochemistry* **37** (1998), 5654–5665.